Resistive evolution of toroidal field distributions and their relation to magnetic clouds

Smiet, C.B.; Blank, H.J.; Jong, T.A. de; Kok, D.N.L.; Bouwmeester, D.

Resistive evolution of toroidal field distributions and their relation to magnetic clouds

C. B. Smiet[1,2,†], H. J. de Blank[3], T. A. de Jong[2], D. N. L. Kok[2] and D. Bouwmeester[2,4]

[1]Princeton Plasma Physics Laboratory, Princeton University, Princeton, NJ, USA

[2]Huygens-Kamerlingh Onnes Laboratory, Leiden University, P.O. Box 9504, 2300 RA Leiden, The Netherlands

[3]DIFFER – Dutch Institute for Fundamental Energy Research, De Zaale 20, 5612 AJ Eindhoven, the Netherlands

[4]Department of Physics, University of California Santa Barbara, Santa Barbara, CA 93106, USA

We study the resistive evolution of a localized self-organizing magnetohydrodynamic equilibrium. In this configuration the magnetic forces are balanced by a pressure force caused by a toroidal depression in the pressure. Equilibrium is attained when this low-pressure region prevents further expansion into the higher-pressure external plasma. We find that, for the parameters investigated, the resistive evolution of the structures follows a universal pattern when rescaled to resistive time. The finite resistivity causes both a decrease in the magnetic field strength and a finite slip of the plasma fluid against the static equilibrium. This slip is caused by a Pfirsch–Schlüter-type diffusion, similar to what is seen in tokamak equilibria. The net effect is that the configuration remains in magnetostatic equilibrium whilst it slowly grows in size. The rotational transform of the structure becomes nearly constant throughout the entire structure, and decreases according to a power law. In simulations this equilibrium is observed when highly tangled field lines relax in a high-pressure (relative to the magnetic field strength) environment, a situation that occurs when the twisted field of a coronal loop is ejected into the interplanetary solar wind. In this paper we relate this localized magnetohydrodynamic equilibrium to magnetic clouds in the solar wind.

Key words: astrophysical plasmas

---

1. Introduction

Spontaneous self-organization of magnetized plasma lies at the basis of many fascinating phenomena in both fusion reactor operation and astrophysical plasma observations. In such situations, magnetic helicity in the plasma is of crucial importance in determining the evolution of the system. Magnetic helicity is an integral quantity calculated by $H_m = \int \boldsymbol{A} \cdot \boldsymbol{B} \, \mathrm{d}^3 x$ where $\boldsymbol{A}$ is the vector potential and $\boldsymbol{B} = \nabla \times \boldsymbol{A}$ is the magnetic field. Helicity was given its name by Moffatt (1969) who

† Email address for correspondence: csmiet@pppl.gov

recognized its topological interpretation; a measure of the self- and interlinking of magnetic field lines. This notion was extended to non-closing and ergodic field lines by Arnol'd (1986). In a perfectly conducting plasma, the magnetic field can be seen as being 'frozen in' and is advected with the fluid motion (Alfvén 1943; Batchelor 1950). Since the fluid motions can then only distort and reshape the magnetic field lines, but cannot break or cause unlinking, the conservation of helicity is easily understood from a topological perspective.

In perfectly conducting plasma helicity is exactly conserved (Berger & Field 1984), whilst in resistive plasma the rate of energy decay is strongly constrained by its presence (Del Sordo, Candelaresi & Brandenburg 2010). The most famous example where helicity determines a self-organizing process is the Taylor conjecture (Taylor 1974, 1986) which states that the magnetic field in a toroidally bounded plasma relaxes to a linear force-free state (shown by Woltjer (1958) to be the lowest-energy state) with exactly the same helicity as it started with.

But what state is achieved when a helical plasma relaxes in an environment without a boundary? If the plasma's fluid pressure is high compared to the magnetic pressure (high plasma $\beta = p/(B^2/2)$), the linking in the initial field gives rise to a self-organized magnetohydrodynamic (MHD) equilibrium where field lines lie on nested toroidal magnetic surfaces (Smiet *et al.* 2015). The approximately axisymmetric field is in a Grad–Shafranov equilibrium (Shafranov 1966), and the Lorentz force is balanced by a gradient in pressure. The pressure is lowest on the magnetic axis, which is the field line lying at the centre of the nested toroidal magnetic surfaces. In this structure the rotational transform is nearly constant from surface to surface. As a consequence the magnetic field line structure is topologically similar to the mathematical structure of the Hopf fibration (Hopf 1931) or its generalization to torus knots (Arrayás & Trueba 2014; Smiet *et al.* 2015). It should be noted that the Hopf structure has previously also been used in a beautiful paper by Finkelstein and Weil (Finkelstein & Weil 1978) to generate linked and knotted magnetic fields for astrophysics. The relaxation of the Hopf field to the Grad–Shafranov equilibrium has been shown using topology conserving relaxation in our recent paper (Smiet, Candelaresi & Bouwmeester 2017). It is remarkable that this structure is obtained for a wide class of initially helical fields; it emerges from trefoils (Smiet *et al.* 2015), twisted rings and even Borromean linked flux tubes (Candelaresi & Brandenburg 2011).

The robust generation of this ordered magnetic structure makes it natural to assume that a similar process emerges after the twisted magnetic field of a coronal loop is ejected into the high-β interplanetary plasma of the solar wind. The pressure in the solar wind at 1 A.U. is of the order of $p = 1.4 \times 10^{-11}$ N m^{-2} and the field strength $B = 6 \times 10^{-9}T$ such that the plasma $\beta = 2\mu_0 p/B^2 \simeq 1$ (Goedbloed & Poedts 2004). Such events are called coronal mass ejections (CMEs), and CMEs are correlated with the observation of magnetic clouds (Burlaga 1991). A magnetic cloud is a localized magnetic structure in the interplanetary plasma with increased magnetic field strength, and where the direction of the field varies by a large angle (Burlaga 1991). These magnetic signatures are observed by interplanetary satellites with increasingly accurate magnetic instruments (Raghav & Kule 2018). Unfortunately due to the low density of probes in the interplanetary medium, high-resolution measurement of the complete magnetic structure in these clouds is challenging.

There are several models for the magnetic structure of these clouds published in the literature (Burlaga 1991). Some models assume the field in the cloud is still magnetically connected to the surface of the Sun, but there are several models that assume a localized magnetic field which is created by internal currents and balanced by the external plasma pressure (Ivanov & Harshiladze 1985; Burlaga 1991;
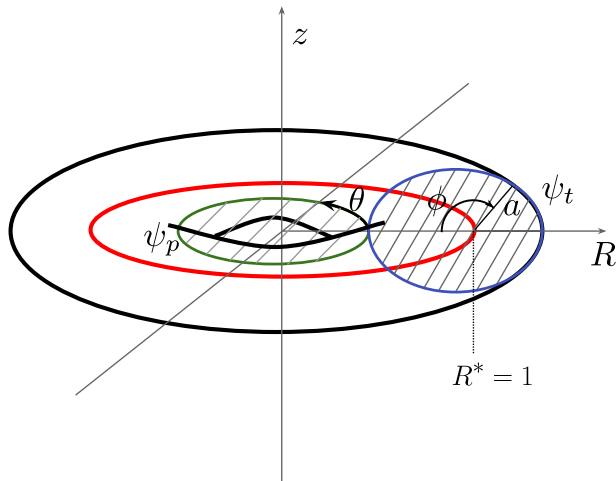
FIGURE 1. Coordinate system used for the construction of the initial magnetic field. The surfaces through which the toroidal flux ψ_t and poloidal flux ψ_p are defined are shown by the blue and green circles respectively; ϕ is the coordinate pointing in the poloidal direction of the torus, and θ is the coordinate pointing in the toroidal direction. The magnetic axis is given by the red circle located at $R^* = 1$.

Vandas *et al.* 1992; Garren & Chen 1994; Kumar & Rust 1996). In this paper we posit the self-organized state identified in Smiet *et al.* (2015) as a new model. This model gives different predictions for the structure from the models above.

In this paper, we study the evolution of the self-organizing equilibrium starting from a twisted flux tube. We vary both the resistivity of the simulation as well as the amount of twist in the initial flux tube. The evolution of the structure is governed by two processes. First, the lowering of the magnetic field strength changes the equilibrium condition, such that the depression in pressure becomes smaller. Second, finite resistance breaks the frozen-in condition, allowing the plasma fluid to slip perpendicular to the magnetic field lines of the configuration. The net effect of this is a fluid flow directed towards the region of lowest pressure. The combined effect of these two processes is a structure that grows on a resistive time scale. The magnetic topology, characterized by the rotational transform of the magnetic surfaces, quickly reaches a nearly flat profile with a slight positive curvature. The rotational transform decays according to a power law, the characteristic exponent of which depends on the aspect ratio of the structure.

2. Initial field

In our previous paper (Smiet *et al.* 2015), we showed how a self-organizing equilibrium is generated through the chaotic reconnection of linked magnetic flux rings. The violent reconnection and high spatial gradients generated when the flux tubes meet, necessitated a high value of resistivity and low magnetic field strength to numerically resolve.

In this paper we use an initial condition which reorganizes in a much more ordered fashion. The initial field consists of a twisted flux tube with field lines lying on nested toroidal flux surfaces with varying rotational transform. We use cylindrical coordinates R, z, θ and flux functions $\psi_p(R, z)$ and $I(\psi_p)$. The coordinate system is described in figure 1. Physically $\psi_p(R, z)$ represents the poloidal magnetic flux, passing through a

circular surface of radius R around the z-axis (green circle). I physically represents the total poloidal current, the current through the green, shaded circle. The magnetic field is calculated from the flux functions by the standard methods for axisymmetric fields (Goedbloed, Keppens & Poedts 2010):

$$B_R = -\frac{1}{R}\frac{\partial \psi_p}{\partial z}, \quad B_z = \frac{1}{R}\frac{\partial \psi_p}{\partial R}, \quad B_\theta = \frac{1}{R}I. \tag{2.1a-c}$$

Using this construction guarantees that the magnetic field is divergence free, and that field lines lie on magnetic surfaces of constant ψ_p.

We choose the following flux function,

$$\psi_p = \begin{cases} B_0 \cos^4 \left(\frac{\pi}{2}\frac{a}{a_0}\right), & a \leqslant a_0 \\ 0, & a > a_0, \end{cases} \tag{2.2}$$

where $0 < a_0 < 1$ and with B_0 a scaling parameter that sets the magnetic field strength and

$$a = \sqrt{(1-R)^2 + z^2}, \tag{2.3}$$

denoting the distance from the unit circle (the circle $R = 1, z = 0$, indicated in red in figure 1), which is the magnetic axis of this initial condition.

With this choice we can see that ψ_p is constant and zero for $a \geqslant a_0$ such that, according to (2.1), the poloidal field vanishes. The magnetic surfaces in the region where $a < a_0$ form concentric tori with circular cross-section that enclose the magnetic axis.

We can choose any function of ψ_p for the toroidal current function I, which here we define as:

$$I = \frac{\psi_p \pi^2}{\iota_0^* a_0^2}, \tag{2.4}$$

where a scaling parameter ι_0^* is introduced, named such because it sets the rotational transform on axis, as we will show in §2.1. With this choice for I the toroidal magnetic field also vanishes for $a \geqslant a_0$, and thus the field describes an axisymmetric flux tube with major radius 1 and minor radius a_0 with $\boldsymbol{B} = 0$ outside of the tube. *Note:* we use the convention that a subscript zero denotes a value at time $t = 0$, and a superscript asterisk denotes that the quantity is measured on the magnetic axis.

2.1. *Rotational transform profile*

The winding of field lines in a toroidal magnetic structure is quantified by the rotational transform ι or its inverse, the safety factor q. The rotational transform geometrically represents the ratio of the number of times a field line wraps around the poloidal direction of a torus to the number of times it winds around the toroidal direction. The safety factor can be calculated using the well-known formula (Wesson & Campbell 2011):

$$q = \frac{1}{2\pi} \oint \frac{1}{R}\frac{B_\theta}{B_p} \, dl, \tag{2.5}$$

where B_p is the magnitude of the poloidal magnetic field $B_R \hat{R} + B_z \hat{z}$, and the integration is carried out over a constant θ cross-section of a magnetic surface ($\psi_p = $ const.). This integration path is indicated by the blue circle in figure 1.

The poloidal magnetic flux enclosed between concentric magnetic surfaces of radii a and $a + \mathrm{d}a$ is $\mathrm{d}a 2\pi R B_p$. Hence conservation of poloidal flux implies that RB_p is constant on each surface. Evaluating the poloidal field at $z = 0$, $R \geqslant 1$, where $\partial \psi_p / \partial z = 0$ and $\partial \psi_p / \partial R = \partial \psi_p / \partial a$ its value in the direction of the poloidal vector $\boldsymbol{\phi}$ is equal to

$$RB_p = \frac{\partial \psi_p}{\partial a} = B_0 \frac{2\pi}{a_0} \cos^3 \left(\frac{a\pi}{2a_0} \right) \sin \left(\frac{a\pi}{2a_0} \right). \tag{2.6}$$

The toroidal magnetic field is:

$$B_\theta = B_0 \frac{\pi^2 \cos^4 \left(\dfrac{\pi a}{2a_0} \right)}{R \iota_0^* a_0^2}. \tag{2.7}$$

On the magnetic surfaces the parameter a is a constant, so filling this in (2.5) becomes:

$$q(a) = \frac{\cos \left(\dfrac{a\pi}{2a_0} \right)}{4\iota_0^* a_0 \sin \left(\dfrac{a\pi}{2a_0} \right)} \oint \frac{1}{R} \, \mathrm{d}l. \tag{2.8}$$

Using $\boldsymbol{\phi}$ to parametrize the integral over the surface at a, and the identities $R = 1 + a \cos(\boldsymbol{\phi})$ and $\mathrm{d}l = a \, \mathrm{d}\boldsymbol{\phi}$, we get:

$$\oint \frac{1}{R} \, \mathrm{d}l = \int_0^{2\pi} \frac{a}{1 + a \cos(\boldsymbol{\phi})} \, \mathrm{d}\boldsymbol{\phi} = \frac{2\pi a}{\sqrt{1 - a^2}}. \tag{2.9}$$

This gives us the safety factor

$$q(a) = \frac{\dfrac{a\pi}{2a_0} \cot \left(\dfrac{a\pi}{2a_0} \right)}{\iota_0^* \sqrt{1 - a^2}}, \tag{2.10}$$

and hence a rotational transform of:

$$\iota(a) = \iota_0^* \sqrt{1 - a^2} \frac{\tan \left(\dfrac{a\pi}{2a_0} \right)}{\dfrac{a\pi}{2a_0}}. \tag{2.11}$$

The rotational transform profile is flat near the magnetic axis, and increases to infinity when $a \to a_0$. At the magnetic axis the rotational transform is given by

$$\lim_{a \to 0} \iota(a) = \iota_0^*. \tag{2.12}$$

The initial condition is thus an axisymmetric, twisted magnetic flux tube lying in the R, θ-plane. We can change the twist of the magnetic field lines in the initial condition by tuning the parameter ι_0^*, and the toroidal magnetic field strength with the parameter B_0.

3. Time evolution

We simulate the time evolution of the helical magnetic fields numerically using the resistive, viscous, compressible isothermal MHD equations. The equations are solved using the PENCIL-CODE (http://pencil-code.nordita.org/). This is a highly used solver of the MHD equations on a fixed Eulerian grid often used for astrophysical applications (Brandenburg & Dobler 2002; Haugen, Brandenburg & Dobler 2004; Johansen *et al.* 2007).

The PENCIL-CODE solves the MHD equations in terms of the vector potential A, ensuring that the magnetic field remains divergence free. The equation of motion solved is:

$$\frac{Dv}{Dt} = -c_s^2 \nabla \ln \rho + j \times B/\rho + F_{\text{visc}}/\rho, \tag{3.1}$$

where B is calculated through $B = \nabla \times A$ and the current $j = \nabla \times B$. The fluid velocity is v and the convective derivative is denoted by $D/Dt \equiv (\partial/\partial t) + v \cdot \nabla$. The simulation is isothermal, so the pressure is related to the density by $p = \rho c_s^2$ where c_s^2 is the sound speed (set to unity). The viscous force F_{visc} is calculated using the rate of strain tensor S whose indices are given by $S_{ij} = (1/2)(\partial u_i/\partial x_j + \partial u_j/\partial x_i) - (1/3)\delta_{ij} \nabla \cdot v$. through the equation:

$$F_{\text{visc}} = \nabla \cdot 2\nu\rho S. \tag{3.2}$$

The continuity equation is implemented in terms of the logarithm of the density ρ as follows

$$\frac{D \ln \rho}{Dt} = -\nabla \cdot v. \tag{3.3}$$

Since the plasma is modelled as isothermal the equation of state does not need to be solved, so the final equation is the induction equation, which in terms of the vector potential becomes

$$\frac{\partial A}{\partial t} = v \times B + \eta \nabla^2 A, \tag{3.4}$$

where we have chosen the Weyl gauge for A to simplify the equation and η is the resistivity.

These equations are solved on an Eulerian grid of 256^3 grid points in a simulation box of size 5. This puts the boundary at $R = 2.5$. The simulation is run using perpendicular-field boundary conditions, by imposing a vanishing parallel component of the magnetic field on the boundary. This boundary condition allows magnetic field to escape from the simulation volume. The full field information is saved every 5 simulation time steps. The simulation is initialized with a constant pressure $p = 1$ throughout the volume and the velocity field is zero. The Alfvén speed v_A in the initial field ranges from 0.28 to 1.1 (on axis) B_0 is varied between 0.05 and 0.2 and this makes it of the same order of magnitude as the sound speed $c_s^2 = 1$. We scale the time to a resistive time scale using $t_\eta = R_{\text{char}}^2/\eta$. For the characteristic length scale R_{char} we choose the distance of the magnetic axis from the origin in the initial field, $R^*(0) = 1$. The viscosity parameter ν is set to 2×10^{-4} whereas the resistivity η is varied from 2×10^{-4} to almost an order of magnitude lower. This makes the magnetic Prandtl number equal to unity or larger.

In our analysis of the simulation results we wish to extract the topological properties of the magnetic field structures. We do this by means of a Runge–Kutta field line integration. From the resultant field line traces we can find the magnetic axis and the rotational transform of the field line if it lies on a toroidal surface. One implementation of this field line tracing is described in the supplemental material of Smiet *et al.* (2015). This method was used in §§ 4 and 5.
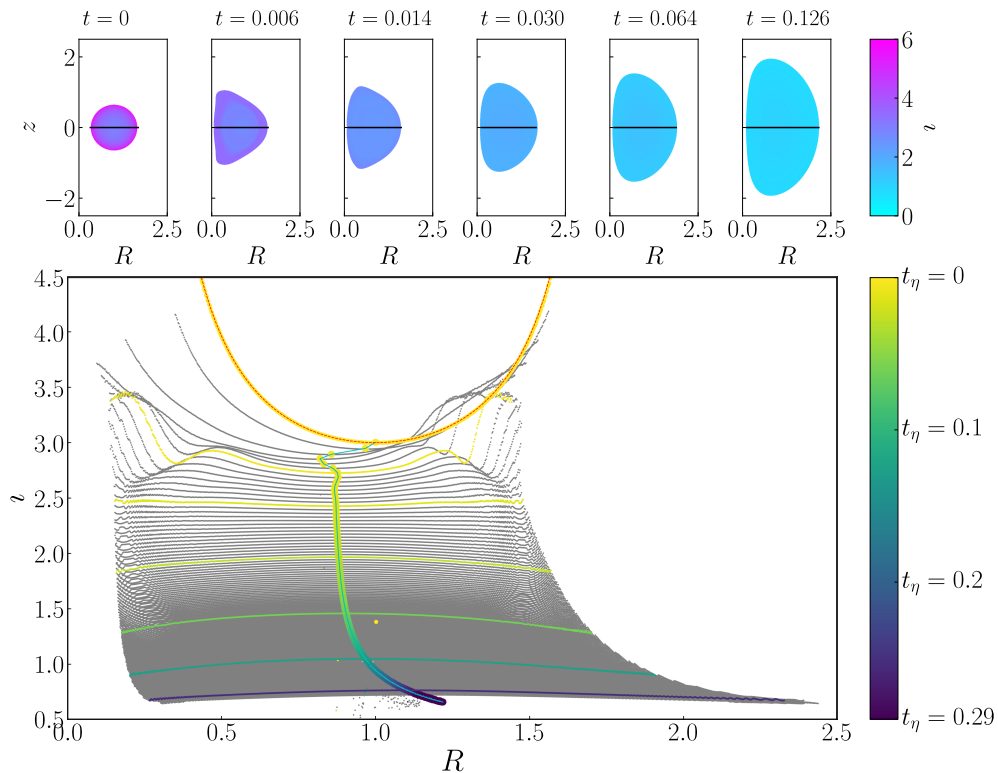
FIGURE 2. Resistive evolution of the magnetic structure. Parameters are: $\iota_0^* = 3$, $B_0 = 0.05$ and $\eta = 2 \times 10^{-4}$. (*a*) Cross-sections in the R, z-plane at different times. The colour indicates the rotational transform of a field line starting at that position. The configuration is seen to first contract onto the z-axis and then slowly expand. The horizontal lines indicates the location where the rotational transform, shown in (*b*), is taken. The cross-sections shown are at times which correspond with the top six coloured lines in (*b*) and are exponentially spaced. (*b*) Evolution of the rotational transform profile and the location of the magnetic axis. The black line along the centre is the location of the magnetic axis. The coloured part around the black line indicates the time at which the magnetic axis was at that location. The top six coloured lines correspond to the six cross-sections shown in (*a*), and their colour again indicates the time at which that rotational transform profile was calculated. The red dashed line is the analytical result of (2.11). We can see that the configuration quickly reaches a nearly flat rotational transform profile and subsequently evolves self-similarly.

Furthermore we have developed an alternative implementation in the parallel computing platform CUDA to run on graphics hardware. The hardware accelerated trilinear interpolation and massive parallelization allow for a high speed up compared to CPU-based field line tracing. This code has been made publicly available (de Jong, Kok & Smiet 2018). In the $(R, 0, z)$-plane field lines are traced from a 1024×1024 grid and for every field line the rotational transform is calculated.

The evolution of the rotational transform profile can be seen in supplemental movie 1 available at https://doi.org/10.1017/S0022377818001290. This video shows the colour-coded rotational transform, similar to figure 2(*a*), for all times sequentially. Additionally, this video gives a good indication of how the magnetic structure evolves in time.
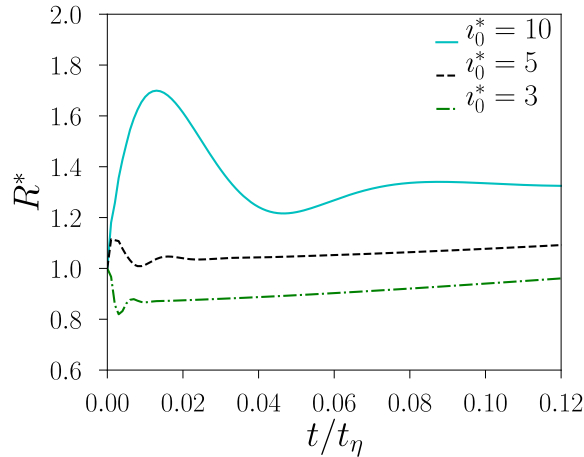
FIGURE 3. Position of the magnetic axis in time for different values of ι_0^*. The magnetic axis performs a damped oscillatory motion towards an equilibrium position which depends on the initial rotational transform, and then slowly grows. The parameters $B_0 = 0.05$ and $\eta = 2 \times 10^{-4}$ are fixed with ι_0^* varied as shown.

The results of this analysis are shown in figure 2(*a*), for the field with $\iota_0^* = 3$, $B_0 = 0.05$ and $\eta = 2 \times 10^{-4}$. Every single pixel in these images is the result of calculating the rotational transform of a field line trace. In this run the magnetic field remains axisymmetric and the magnetic axis remains in the plane defined by $z = 0$. This is the case for all runs presented in this paper, even though these symmetries are in no way enforced by the computational procedure. With higher values of ι_0^* the structure can become susceptible to a non-axisymmetric kink instability, which will be the subject of a future publication.

Figure 2(*b*) shows the rotational transform profile at different times during the evolution of the configuration. The rotational transform profile quickly shifts from positively curved to nearly flat with a slight negative curvature. After this initial phase the rotational transform profile remains nearly constant in space but decreases in time. In the next sections we will study this decay.

In the rest of the paper we will analyse the change in rotational transform and the location of the magnetic axis in time. We will look at the effect of changing the resistivity η and the initial rotational transform ι_0^*.

4. Resistive growth and decay of rotational transform

In figure 2 it is seen that the magnetic axis first shifts inwards and then slowly moves back out. We follow this dynamic of the magnetic structure by extracting R^*, the distance from the origin to the magnetic axis as a function of resistive time. This is done for three different values of ι_0^* at constant $\eta = 4 \times 10^{-4}$. The results are shown in figure 3. The structure relaxes to a radius which depends on ι_0^*, and then slowly increases in size.

As the structure grows, it has reached its equilibrium: the magnetic pressure pushes outwards, but the expansion is halted by the strong external pressure. A lowering of the pressure is observed in a toroidal region as we show here in figure 6, and is described in more detail in Smiet *et al.* (2015, 2017).
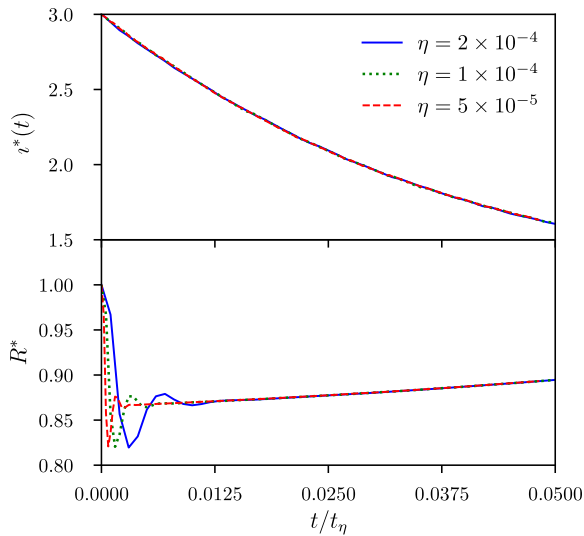
FIGURE 4. Values of $\iota^*(t)$ and $R^*(t)$ as functions of resistive time for several different values of resistivity η. The initial rotational transform is set to $\iota_0^* = 3$, and magnetic field strength $B_0 = 0.05$. The change of the rotational transform and the radius of the structure all behave identically on a resistive time scale.

We can understand this initial relaxation qualitatively from the interplay between magnetic tension and magnetic pressure. Since the initial pressure is constant and the velocity is zero the initial motion of the fluid is purely due to the Lorentz force $\boldsymbol{j} \times \boldsymbol{B}$. A high value of ι_0^* results in a high poloidal field, and magnetic tension along the field lines squeezes the configuration into an expanding ring. The case of a low rotational transform will result in stronger toroidal field, and the magnetic tension will cause the structure to contract. In figure 3 we see that higher ι_0^* leads to an initial expansion, and an equilibrium with a value of R^* larger than 1, whereas low values of ι_0^* lead to an initial contraction. R^* performs a damped Alfvénic oscillation to the equilibrium position, and then slowly grows.

The later evolution of the structure proceeds on a purely resistive time scale. This is tested by simulating the evolution of the field with the parameters $\iota_0^* = 3$, $B_0 = 0.05$ and varying resistivity $\eta = 2 \times 10^{-4}$, 1×10^{-4} and 5×10^{-5}. When rescaled to resistive time the growth of the structure and the change in rotational transform all collapse to a single curve indicating a universal growth mechanism, as shown in figure 4.

The magnetic field strength B_0 does not affect the equilibrium reached or the rate of growth and change in rotational transform exhibited by these configurations. This is shown in figure 5, where the fields with $B_0 = 0.05$ and $B_0 = 0.2$ are compared for $\iota_0^* = 3$, $\eta = 2 \times 10^{-4}$. Despite a factor 4 difference in the magnetic field strength the structures behave identically except for the initial reconfiguration towards the equilibrium. As this reconfiguration is mediated by magnetic forces, it proceeds on an Alfvénic time scale linear in the magnetic field, $\tau_A = B/\sqrt{\rho}$. It is therefore not surprising that the oscillation to the equilibrium R^* lasts approximately 4 times longer for the field where the magnetic amplitude is a quarter of the strength.

5. Pfirsch–Schlüter diffusion

We can understand the structure growth and change in rotational transform through the effect of finite resistivity on the plasma and the lowering of magnetic field
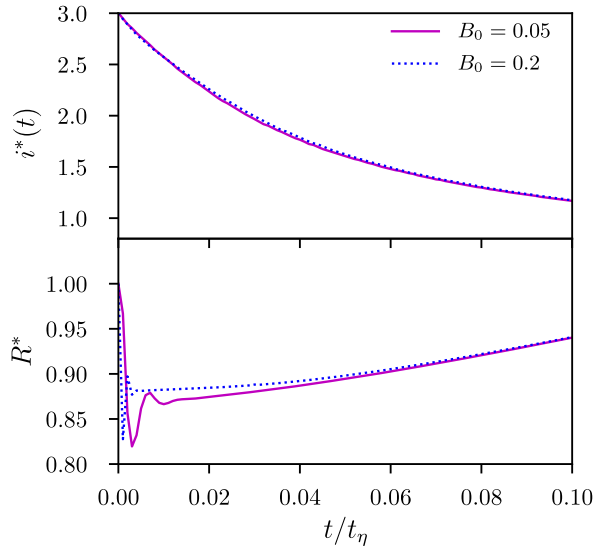
FIGURE 5. Magnetic decay of topologically identical structures with different initial magnetic field strength B_0. Despite the difference in magnetic field strength the change in rotational transform proceeds at exactly the same rate with identical equilibrium. Note that the initial oscillations towards the equilibrium radius occur on the Alfvénic time scale: the oscillations to the equilibrium configuration proceed at a four times faster rate when $B_0 = 0.2$ then when $B_0 = 0.05$. In these runs $\iota_0^* = 3$ and $\eta = 2 \times 10^{-4}$.

strength through resistivity. In a perfectly conducting plasma a magnetic field is effectively 'frozen-in' and moves with the fluid motion (Alfvén 1943; Batchelor 1950; Priest & Forbes 2000), thus there can be no net flow of fluid perpendicular to the field lines if the magnetic configuration is static. When resistivity is included this restriction is lifted and the fluid can slip against the static magnetic field lines. Field line slip is observed in many different scenarios and is one of the driving mechanisms behind two-dimensional reconnection (Kulsrud 2011). In the toroidal geometry of an operating tokamak, field line slip gives rise to slow diffusion out of the toroidal flux surfaces. This process is called Pfirsch–Schlüter diffusion (Wesson & Campbell 2011). This Pfirsch–Schlüter flow is directed outwards, in the direction of the pressure gradient.

In the self-organized structures considered here a similar magnetic slip causes a diffusion of plasma fluid into the magnetic structure. This is shown in figure 6, where the flow field is plotted along the x-axis together with the pressure profile. The magnetic axis is located at the minimum of the pressure, and it is clearly seen how there is net fluid flow directed towards the magnetic axis. We suggest that the slight discrepancy between the location of the magnetic axis and the zero of the velocity is due to the axis itself being in motion.

Whilst the fluid flow slowly penetrates the magnetic structure, the magnetic energy in the structure is decreasing. The decrease of total magnetic energy for the simulations with $\iota_0^* = 3$ and $B_0 = 0.05$ is shown in figure 7.

One important result to note is that the magnetic field strength decays fast compared to the resistive decay time t_η, whereas in general the magnetic field strength is expected to evolve as $\langle |\boldsymbol{B}| \rangle \sim \langle B_0 \rangle e^{-t/t_\eta}$. Here the magnetic energy has already decreased an order of magnitude in only $0.1 t_\eta$. This is because the resistive losses
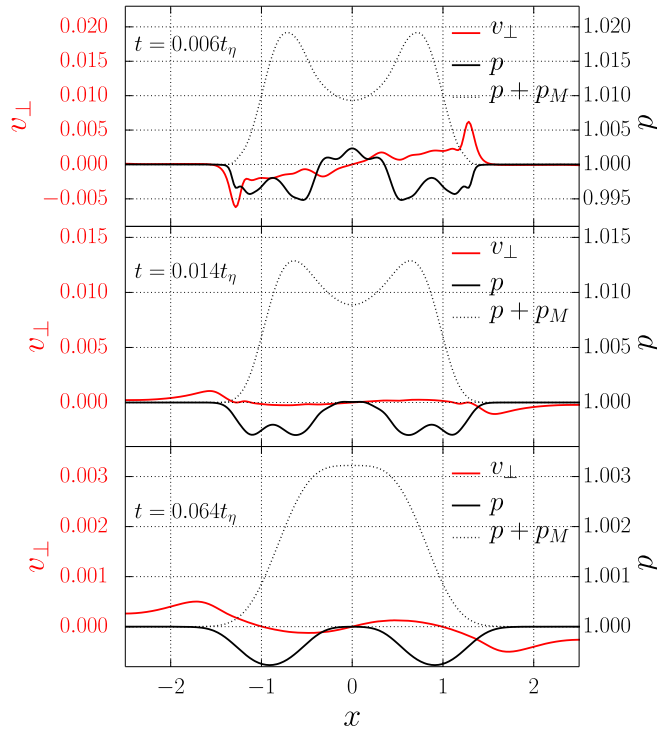
FIGURE 6. Fluid velocity $v_\perp$ (red), pressure p (black) and total pressure $p + p_M$ along the x-axis at three different times corresponding to the second, third and fifth images in figure 2(a). The resistivity of this run was $\eta = 2 \times 10^{-4}$ and $\iota_0^* = 3$. During the initial reconfiguration, the pressure profile is irregular, but the total pressure is smooth. In (c), the equilibrium has reached the state where the magnetic axis is located at the minimum in pressure. The flow profile shows a net flow towards the magnetic axis which is similar to Pfirsch–Schlüter diffusion.
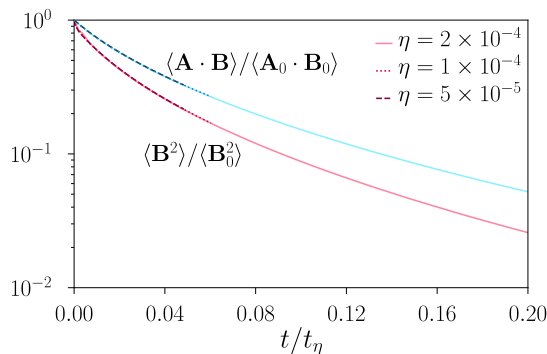

FIGURE 7. Decay of magnetic energy and decay of total helicity versus time for the runs with $\iota_0^* = 3$ and $B_0 = 0.05$ for different values of resistivity η.

are not the only mechanism through which the magnetic field is lowered: during the evolution the entire configuration also expands. Even with zero resistivity such an expansion leads to a lowering of the magnetic field strength. This can be seen as
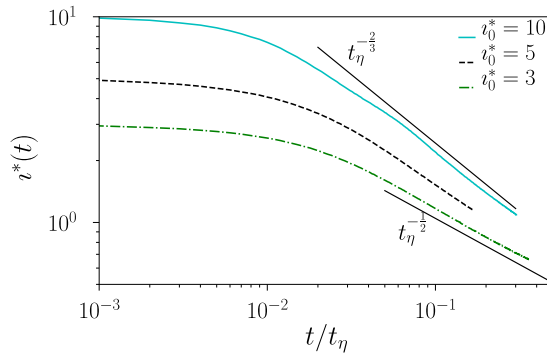
FIGURE 8. Time dependence of the rotational transform for different values of ι_0^*. After the initial period where the magnetic structure reorganizes on an Alfvénic time scale, the rotational transform decays following a power law with a characteristic exponent between $-2/3$ and $-1/2$.

follows: since it is the flux through a co-moving surface that is conserved, and if that surface expands, the magnetic field strength lowers. This effect can also be seen in the zero resistance simulations presented in (Smiet *et al.* 2017).

Figure 7 also shows the evolution of magnetic helicity, which decreases at a slower rate than the magnetic energy. The slower decay of helicity can be seen as the result of the expansion, as the structure evolves with a self-similar shape. The magnetic energy is the integral of $(\nabla \times A) \cdot (\nabla \times A)$, whereas the integrand of the helicity integral, $A \cdot (\nabla \times A)$, involves one less spatial derivation. For a similar structure of a larger size, the magnetic helicity is thus larger. Note that we evolve these structures on a time scale larger than the time scales on which the helicity can be considered conserved, and that our initial condition is intentionally very regular. Therefore the localized reconnections which transform helicity between linking, writhe and twist, which reconfigure the magnetic topology whilst leaving helicity mostly unchanged in turbulent Woltjer–Taylor-type relaxation, are absent in these runs. See Smiet *et al.* (2015) for simulations where this equilibrium is achieved through this more chaotic reconnection.

Finally, we look at the change of rotational transform in time, and how it depends on the initial value for the rotational transform. The results are shown in figure 8. From the asymptotic behaviour in the log–log plot we can see that the rotational transform decays according to a power law instead of exponentially. The characteristic exponent of this decay is different for runs with different ι_0^*. The rotational transform between $t_\eta = 0.05$ and $t_\eta = 0.1$ is fitted with a power law $\iota^*(t) = at_\eta^{-b}$ and a characteristic exponent of $b = 0.664$ is found for the run with $\iota_0^* = 10$ and $b = 0.48$ for the run with $\iota_0^* = 3$. Guides are drawn in figure 8 showing $t_\eta^{-2/3}$ and $t_\eta^{-1/2}$ decay.

The lowering rotational transform is caused by the poloidal field decreasing faster than the toroidal field. This is another indication that the lowering of field strength is primarily caused by the expansion of the structure caused by field line slip and not necessarily by resistive decay. With resistive decay we indicate the exponential decay with characteristic decay time t_η caused by resistivity on a static field configuration, solutions of (3.4) with $v = 0$. Decay brought on by field line slip is caused by the non-zero Pfirsch–Schlüter flow, or conversely the motion of the field lines against the plasma. This causes the term v to be non-zero and the term $\nabla^2 A$ to decrease

(through expansion the gradients get smaller) in (3.4), and thus the change in magnetic field strength can be fast compared to the resistive decay time.

As the structure expands the poloidal field strength is lowered by expansion in the horizontal plane, as it is the poloidal flux passing through the circle defined by the magnetic axis which is conserved. The increase in area through which this flux passes is proportional to $(R^*)^2$. The lowering of the toroidal field meanwhile is governed by the change in area of the poloidal cross-section of the flux tube. Expansion in this plane is constrained to the positive R-direction and as such the area should go approximately linear in R^*. This constrained expansion is attested by the D-shaped magnetic surfaces seen in figure 2(*a*). Even though this explanation is quite qualitative and does not take into account the shape of the surfaces and the distribution of magnetic flux, it does explain why the rotational transform lowers according to a power law. Furthermore, the difference between poloidal and toroidal expansion correctly predicts a characteristic exponent of around $-1/2$.

It should be noted that the decay in rotational transform is fast compared to the increase of the major radius of the structure; the rotational transform changes by a factor of three in the time R^* only changes a few per cent. This is important when considering this equilibrium as a model for magnetic clouds.

6. Relation to magnetic clouds

The presented simulations of axisymmetric equilibria are more idealized than the situation encountered in the solar wind. As noted in the introduction, the plasma β in the solar wind is approximately 1, and a signature of a magnetic cloud is that the β drops below 1 (Zurbuchen & Richardson 2006). In these simulations, the initial β (taking the magnetic field strength and pressure on the axis) is approximately 25 when $B_0 = 0.05$ and 1.65 when $B_0 = 0.2$. However, as can be seen from figure 5, when rescaled to resistive time the evolution of the fields is near identical. Simulations (not presented in this paper) have been performed at β down to 0.7 which show the same evolution, but this is not a lower limit. The simulations show the set-up of a toroidal equilibrium against a background plasma with lower field strength, similar to the situation encountered in the solar wind.

In the solar wind the Alfvén speed and the sound speed are the same order of magnitude with $v_s = 37$ km s^{-1} and $v_A = 47$ km s^{-1} (Goedbloed & Poedts 2004). Assuming a magnetic cloud size of approximately 10^6 km (1 day passage for a probe travelling at 15 km s^{-1}), the Alfvénic transit time is approximately 7 h, so one dozen to several dozen Alfvén transit times pass between coronal mass ejection and observation, a similar regime as is probed in the simulation. The magnetic Prandtl number (ratio of kinematic viscosity to magnetic diffusivity) for a hot thin plasma such as the interplanetary solar wind is much higher than unity; $\sim 10^{14}$ (see Brandenburg & Subramanian 2005). The plasma in the solar wind is thus in a regime here the viscous forces act faster than the resistivity to allow for a similar self-organizing process as observed in the simulations. One major difference is that t_η for a magnetic cloud is approximately 10^9 years, much longer than the months for which a cloud can be observed before it leaves the solar system. When the cloud is just ejected, R_{char} is smaller and reconnection can occur (it must to trigger the ejection). Furthermore the more chaotic solar wind allows for small-scale reconnection events which increase the effective reconnection rate. Nevertheless, the extent to which the rotational transform changes must be much smaller than the full evolution presented in this paper.

There are several models for magnetic clouds discussed in the literature, see for example Burlaga (1991) for an overview. One of the more common approaches is to model a magnetic cloud as a long flux rope extending from, and still magnetically connected to, the surface of the Sun. Nevertheless there are several models that consider magnetic clouds as localized magnetic excitations within the solar wind, with their magnetic field generated by internal currents.

Kumar and Rust describe a model for a magnetic cloud as an isolated, net current carrying toroidal flux ring (Kumar & Rust 1996). The magnetic field inside the ring is based on the force-free Lundquist solution valid for an infinite cylinder (Lundquist 1950). As they themselves note, this cannot be an exact description, as the toroidal geometry necessitates the existence of a hoop force such as described in Garren & Chen (1994). In this model the plasma current is zero outside of the toroid, but the net current through the toroid is non-zero such that it generates a force-free field in the surrounding plasma.

There are several differences between Kumar and Rust's model and a magnetic cloud as a self-organized structure we describe. Firstly the magnetic field in their model is force free. Such a field is not possible, as they note themselves because a current ring will always experience a hoop force. The rotational transform profile in their model is also very different. In Lundquist solutions the axial and tangential fields (which, when the cylinder is translated to a torus, correspond to the toroidal and poloidal directions respectively) are given by Bessel functions. As such the rotational transform profile changes significantly from the magnetic axis to the edge (Bellan 2000). The magnetic field outside the ring is purely toroidal, which implies that the rotational transform goes to infinity. Even though their model resembles the configuration we describe superficially, the rotational transform profile is drastically different. Our simulations show that the profile quickly flattens.

Another magnetic cloud model which resembles the configurations we observe is the flare-generated spheromak model by Ivanov & Harshiladze (1985) and further explored by Vandas *et al.* (1992). They describe the clouds using the spherical force-free solution of Chandrasekhar & Kendall (1957). The magnetic topology in this solution also consists of field lines lying on nested toroidal surfaces. In this model the rotational transform profile of these force-free solutions is also non-constant.

The resistive decay time for a structure with the characteristic length scale that is reasonable for magnetic clouds, $R_{char} = 10^6$ km, is approximately 1.7×10^9 years (Goedbloed & Poedts 2004), so change in the rotational transform due to resistive processes is expected to be small. The process leading to the formation of the self-organized localized equilibrium however takes place on a much faster time scale. Note that not just the Alfvénic oscillation towards equilibrium is fast; as seen in figure 2 much of the change in rotational transform towards equilibrium has already occurred at $0.006 t_\eta$. This change, though fast, scales with resistivity. If the resistivity is many orders of magnitude lower, as in the solar wind, this change in rotational transform can be expected to be much less rapid, and the cloud will still carry much of the topology it organized into when it was ejected. The evolution of the magnetic structure, after it is generated, can therefore be considered to be approximately ideal, as is also assumed in the model by Ivanov and Harshiladze and the model by Kumar and Rust.

Because the structure we describe does not rely on the assumption of force-free fields, an assumption that is not warranted in the $\beta \sim 1$ solar wind plasma, we speculate that the magnetic structures described in this paper are a more realistic model for localized magnetic clouds than the two others described above.

7. Conclusions

In this paper we have shown how a self-organizing equilibrium evolves on a resistive time scale. In agreement with our previous studies we find that the initially twisted flux tube reconfigures on an Alfvénic time scale into an axisymmetric Grad–Shafranov equilibrium characterized by a lowered pressure on the magnetic axis.

In this paper we have described how the configuration evolves subsequently; the major radius R^* grows, and the rotational transform on the magnetic axis $\iota^*(t)$ lowers. The rotational transform profile, which initially had a high positive curvature, quickly evolves to a almost flat and slightly negatively curved profile.

With the exception of the initial reconfiguration which proceeds on an Alfvénic time scale, the evolution is rather independent of the resistivity when scaled to a resistive time scale. The growth of the structure can be understood as a Pfirsch–Schlüter-type slip of the field lines against the plasma fluid background, or conversely the fluid slip against the field.

It is because of this growth of the structure that the magnetic field strength decays faster than the resistive time scale. It is also this growth which allows the poloidal field to decay faster than the toroidal field. We have also given a simple geometrical argument that explains why the decay of the rotational transform behaves as a power law with characteristic exponent of the order of $1/2$.

In this study we have limited ourselves to isothermal (constant resistivity) MHD evolution. The inclusion of temperature would result in a spatial variation of the Spitzer resistivity, which would quantitatively change the exact evolution, but the general aspects of the equilibrium and its evolution are underlined by geometrical principles and would remain unchanged. It is an interesting question whether the generation of a flat rotational transform profile would remain robust under these conditions

These results could help make predictions for the evolution of self-organized magnetic equilibria in nature. In this paper we relate this structure to magnetic clouds. Other applications for this model include ejecta from active galactic nuclei (Braithwaite 2010), and one could possibly devise a scheme for pulsed nuclear fusion power generation in which the plasma is confined in such a magnetic structure, embedded in an extremely high fluid pressure environment. When devising such a scheme it should be important to note that the decay time of the magnetic field strength proceeds on a time scale much faster than the resistive decay time, and as such that the 'confinement' is a very transient phenomenon.

Supplementary movie

Supplementary movie is available at https://doi.org/10.1017/S0022377818001290.

REFERENCES

ALFVÉN, H. 1943 On the existence of electromagnetic-hydrodynamic waves. *Ark. Astron.* **29**, 1–7.

ARNOL'D, V. I. 1986 The asymptotic hopf invariant and its applications. *Sel. Math. Sov.* **5** (4), 327.

ARRAYÁS, M. & TRUEBA, J. L. 2014 A class of non-null toroidal electromagnetic fields and its relation to the model of electromagnetic knots. *J. Phys.* A **48** (2), 025203.

BATCHELOR, G. K. 1950 On the spontaneous magnetic field in a conducting liquid in turbulent motion. *Proc. R. Soc. Lond.* A **201** (1066), 405–416.

BELLAN, P. M. 2000 *Spheromaks: A Practical Application of Magnetohydrodynamic Dynamos and Plasma Self-Organization*. World Scientific.

BERGER, M. A. & FIELD, G. B. 1984 The topological properties of magnetic helicity. *J. Fluid Mech.* **147**, 133–148.

BRAITHWAITE, J. 2010 Magnetohydrodynamic relaxation of agn ejecta: radio bubbles in the intracluster medium. *Mon. Not. R. Astron. Soc.* **406** (2), 705–719.

BRANDENBURG, A. & DOBLER, W. 2002 Hydromagnetic turbulence in computer simulations. *Comput. Phys. Commun.* **147** (1–2), 471–475.

BRANDENBURG, A. & SUBRAMANIAN, K. 2005 Astrophysical magnetic fields and nonlinear dynamo theory. *Phys. Rep.* **417** (1–4), 1–209.

BURLAGA, L. F. 1991 Magnetic clouds. In *Physics of the Inner Heliosphere II*, pp. 1–22. Springer.

CANDELARESI, S. & BRANDENBURG, A. 2011 Decay of helical and nonhelical magnetic knots. *Phys. Rev.* E **84** (1), 016406.

CHANDRASEKHAR, S. & KENDALL, P. 1957 On force-free magnetic fields. *Astrophys. J.* **126**, 457.

DEL SORDO, F., CANDELARESI, S. & BRANDENBURG, A. 2010 Magnetic-field decay of three interlocked flux rings with zero linking number. *Phys. Rev.* E **81** (3), 036401.

FINKELSTEIN, D. & WEIL, D. 1978 Magnetohydrodynamic kinks in astrophysics. *Intl J. Theoret. Phys.* **17** (3), 201–217.

GARREN, D. A. & CHEN, J. 1994 Lorentz self-forces on curved current loops. *Phys. Plasmas* **1** (10), 3425–3436.

GOEDBLOED, J. P., KEPPENS, R. & POEDTS, S. 2010 *Advanced Magnetohydrodynamics: With Applications to Laboratory and Astrophysical Plasmas*. Cambridge University Press.

GOEDBLOED, J. P. & POEDTS, S. 2004 *Principles of Magnetohydrodynamics: With Applications to Laboratory and Astrophysical Plasmas*. Cambridge University Press.

HAUGEN, N. E. L., BRANDENBURG, A. & DOBLER, W. 2004 Simulations of nonhelical hydromagnetic turbulence. *Phys. Rev.* E **70** (1), 016308.

HOPF, H. 1931 Über die Abbildungen der dreidimensionalen Sphäre auf die Kugelfläche. *Math. Ann.* **104** (1), 637–665.

IVANOV, K. & HARSHILADZE, A. 1985 Interplanetary hydromagnetic clouds as flare-generated spheromaks. *Solar Phys.* **98** (2), 379–386.

JOHANSEN, A., OISHI, J. S., MAC LOW, M.-M., KLAHR, H., HENNING, T. & YOUDIN, A. 2007 Rapid planetesimal formation in turbulent circumstellar disks. *Nature* **448** (7157), 1022.

DE JONG, T. A., KOK, D. N. L. & SMIET, C. B. 2018 TAdeJong/plasma-analysis: reference release for citation (Version v0.1). Zenodo. http://doi.org/10.5281/zenodo.2069945.

KULSRUD, R. M. 2011 Intuitive approach to magnetic reconnection. *Phys. Plasmas* **18** (11), 111201.

KUMAR, A. & RUST, D. 1996 Interplanetary magnetic clouds, helicity conservation, and current-core flux-ropes. *J. Geophys. Res.* **101** (A7), 15667–15684.

LUNDQUIST, S. 1950 Magneto-hydrostatic fields. *Ark. fys.* **2** (4), 361–365.

MOFFATT, H. K. 1969 The degree of knottedness of tangled vortex lines. *J. Fluid Mech.* **35** (1), 117–129.

PRIEST, E. R. & FORBES, T. G. 2000 *Magnetic Reconnection: MHD Theory and Applications*. Cambridge University Press.

RAGHAV, A. N. & KULE, A. 2018 The first in situ observation of torsional Alfvén waves during the interaction of large-scale magnetic clouds. *Mon. Not. R. Astron. Soc.* **476** (1), L6–L9.

SHAFRANOV, V. 1966 Plasma equilibrium in a magnetic field. *Rev. Plasma Phys.* **2**, 103.

SMIET, C., CANDELARESI, S., THOMPSON, A., SWEARNGIN, J., DALHUISEN, J. & BOUWMEESTER, D. 2015 Self-organizing knotted magnetic structures in plasma. *Phys. Rev. Lett.* **115** (9), 095001.

SMIET, C. B., CANDELARESI, S. & BOUWMEESTER, D. 2017 Ideal relaxation of the hopf fibration. *Phys. Plasmas* **24** (7), 072110.

TAYLOR, J. 1974 Relaxation of toroidal plasma and generation of reverse magnetic fields. *Phys. Rev. Lett.* **33** (19), 1139–1141.

TAYLOR, J. 1986 Relaxation and magnetic reconnection in plasmas. *Rev. Mod. Phys.* **58** (3), 741.

VANDAS, M., FISCHER, S., PELANT, P. & GERANIOS, A. 1992 Magnetic clouds: comparison between spacecraft measurements and theoretical magnetic force-free solutions. In *Solar Wind Seven*, pp. 671–674. Elsevier.

WESSON, J. & CAMPBELL, D. J. 2011 *Tokamaks,* vol. 149. Oxford University Press.

WOLTJER, L. 1958 A theorem on force-free magnetic fields. *Proc. Natl Acad. Sci. USA* **44** (6), 489–491.

ZURBUCHEN, T. H. & RICHARDSON, I. G. 2006 *In-situ* solar wind and magnetic field signatures of interplanetary coronal mass ejections. In *Coronal Mass Ejections*, pp. 31–43. Springer.